Available online at www.sciencedirect.com
SCIENCE DIRECT®
Catalysis Today 90 (2004) 337–342
CATALYSIS TODAY
www.elsevier.com/locate/cattod

# Photocatalysis of V-bearing rutile on degradation of halohydrocarbons

Anhuai Lu [a,*], Juan Liu [a], Donggao Zhao [b], Yanjun Guo [a], Qiaorong Li [a], Ning Li [a]

[a] *Department of Geology, Peking University, Beijing 100871, China*
[b] *Department of Geological Sciences and Electron Microscopy Center, University of South Carolina, Columbia, SC 29208, USA*

**Abstract**

Natural rutile $TiO_2$ shows photocatalysis on degrading trichloroethylene and tetrachloroethylene. In natural rutile, V, Fe, Cu, etc. substitute for Ti, resulting in lattice distortions and defects. We found that rutile, after heating, quenching and electron irradiation, changes its surface characteristics and photoactivity. The quenched rutile has the highest concentrations of adsorbed water and V on its surface, resulting in high photoactivity. For example, quenching at 1273 and 1373 K significantly improved photoactivity of rutile. The heated rutile also increased the concentration of adsorption water on the surface, e.g., rutile heated to 1273 K improved degradation rate of halohydrocarbons. On the contrary, electron irradiation decreased the concentration of adsorbed water on the rutile's surface, which results in lower degradation rate for trichloroethylene. Therefore, heating and quenching over 1237 K improve the photocatalytic efficiency of the natural V-bearing rutile on degrading halohydrocarbons. The XRD spectra of the rutile samples showed that heating, quenching and electron irradiation did not result in formation of new phases or phase transitions.


*Keywords:* Natural V-bearing rutile; Quenching; Heating; Electron irradiation; Photocatalysis; Halohydrocarbon degradation

## 1. Introduction

Photocatalysis is a catalysis process caused by light irradiation [1]. Fujishima and Honda discovered that $H_2O$ decomposes in a photoelectrolysis cell [2]. Since then, photocatalyst has been investigated and used to purify water polluted with organic materials [3,4]. Lu [5] found that semiconducting minerals, especially oxides and sulfides [6,7], could be used to degrade organic contaminants in the environment. Due to its strong oxidability, nontoxicity, cost effectiveness and long-term photostability, titania $TiO_2$ appears to be the most promising photocatalyst. However, the band gap of pure titania is about 3.0 eV and only a small part of solar light with wavelength shorter than 400 nm can excite $TiO_2$ [8,9]. Strong combination of photo-generated electron–hole pairs also limits photocatalysis of pure titania [10]. To improve photocatalytic efficiency of titania, attempts have been tried to dope anatase, a polymorph of titania, with metals or metal oxides [11–13]. It was found that V-doped anatase has strong photoactivity [14,15]. In addition to doping, heating, quenching and electron irradiation were also used to enhance photoactivity of a catalyst [15–18]. Similar to pure anatase, pure rutile, a second polymorph of $TiO_2$, shows no photoactivity [19]. However, depending on preparation procedure, precursor compound [20], and organic reactant [21], rutile could contain impurity components and thus show some photoactivity. For example, naturally occurred rutile usually contains trace elements such as V and Fe and these elements enhance photocatalysis [15,22]. In this study, we modified properties of natural V-bearing rutile by heating, quenching and electron irradiation and investigated photocatalytic effects of these properties on degradation of halohydrocarbons.

## 2. Samples and experiments

### 2.1. Untreated rutile samples

The natural V-bearing rutile used was from a rutile deposit hosted in basic–ultrabasic rocks. The gangue minerals include apatite, tremolite, actinolite, steatite, chlorite, plagioclase, vermiculite, and sphene. The concentrated ore of 93% rutile was obtained by gravitational-magnetic separation. The rutile is deep red in color with sub-metallic luster and its grain sizes range from 0.1 to 1.0 mm.

* Corresponding author.
*E-mail address:* ahlu@pku.edu.cn (A. Lu).

0920-5861/$ – see front matter © 2004 Elsevier B.V. All rights reserved.
doi:10.1016/j.cattod.2004.04.044

### 2.2. Treated rutile samples

The natural rutile grains were ground to sizes of 70–80 μm. In the heating experiment, the ground rutile samples were heated in air in a muffle furnace at 1273 K for 1 h and then cooled down slowly in air. In the quenching experiment, the rutile samples were heated to 1273 K in a 20 kW muffle furnace for 5 min. The heated samples were then put on a steel board and cooled by airflow of 273 K. Both the heating and quenching experiments were conducted at the Beijing University of Science and Technology. In the irradiation experiment, the rutile samples were irradiated with electron beam from the BF-5 Linear Electron Accelerator at Beijing Normal University. The electron energy and irradiation dosage were 3–5 MeV and 1066 kGy, respectively.

### 2.3. Characterization techniques

Chemical compositions of the rutile were obtained by a JEOL JCXA 733 electron microprobe analyzer (EMPA) at China University of Geosciences (Beijing). Crystal structure of the samples was determined by a Rigaku Bruker D8 Advance powder X-ray diffractometer (XRD) with Cu Kα radiation at Peking University. X-ray photoelectron spectroscopy (XPS) analyses were performed by a PHI-5300/ESCA instrument with a monochromatized Al Kα source under a pressure of $2.92 \times 10^{-7}$ Pa at Tsinghua University. The angle discrimination was 45° and the energy resolution was 0.8 eV. The C 1s line at $284.6 \pm 0.2$ was used for a final energy scale calibration.

### 2.4. Degradation experiment

In the degradation experiment, 0.8 g ground rutile sample, 5 ml 3% $H_2O_2$ solution, and 2–3 ml methanol were added into 700 ml trichloroethylene or tetrachloroethylene aqueous solution of 400 μg/l in a reaction container, which was irradiated by a 8 W mercury lamp. Then the reaction container was put into an oscillator for water bath at a constant temperature. Concentrations of halohydrocarbons were measured at different times using HP-6890 gas chromatography with electron capture detection (ECD). For the purpose of comparison, experiments without rutile were also conducted. The degradation rate (%) of halohydrocarbons at $t$ time is defined as

$$\text{degradation rate} = \left[\frac{c_0 - c_t}{c_0}\right] \times 100\% \quad (1)$$

where $c_0$ and $c_t$ are concentrations of halohydrocarbons at initial time and $t$ time, respectively.

## 3. Results

### 3.1. Compositions and structures of rutile

The chemical compositions of the natural rutile are listed in Table 1. On average the rutile contains 96.49 wt.% $TiO_2$, 1.22 wt.% $V_2O_5$, 0.39 wt.% $Fe_2O_3$, 0.35 wt.% ZnO, and 0.22 wt.% CuO. Radii of six-fold coordinated $V^{5+}$, $Fe^{2+}$ and $Fe^{3+}$ are 0.062, 0.069 and 0.063 nm, respectively, similar to that of $Ti^{4+}$ (0.069 nm) [23]. Therefore, these elements could easily substitute Ti in the rutile structure [24,25]. Most researchers agreed that V-doped anatase has strong photoactivity [14,15]. The V-bearing rutile is a natural counterpart of V-doped $TiO_2$, thus has potential to serve as photocatalyst. In Table 1, contents of toxic elements, such as Pb, Cr, Cd, Hg and As, are low. Therefore, the rutile is also environmentally friendly, causing no further pollution during sample preparation and degradation [5].

The XRD patterns of the treated and untreated rutile samples indicated that all samples are rutile. There is no phase change after the treatments, and no titania phase, $V_2O_5$ or other oxide phases were detected.

### 3.2. Surface features of rutile

XPS analyses were used to study the surface features of rutile, which are important for catalytic activity. Ti 2p spectra of all the samples consist of Ti $2p_{3/2}$ and Ti $2p_{1/2}$ double peaks, and the corresponding binding energies are given in Table 2, which are consistent with the binding energies reported for $Ti^{4+}$ in titanium dioxide (458.5 eV for Ti $2p_{3/2}$ and 464.2 eV for Ti $2p_{1/2}$) [26]. All the Ti $2p_{3/2}$ and Ti $2p_{1/2}$ peaks are sharp and symmetric, and there is no low binding energy shoulder for $Ti^{3+}$ [27,28]. Therefore, Ti valence is +4 in all rutiles.

Table 1
Chemical compositions of the natural rutile (wt.%)

| Rutile | $TiO_2$ | $V_2O_5$ | FeO | CuO | ZnO | $Cr_2O_3$ | CdO | HgO | $As_2O_3$ | $Nb_2O_5$ |
|---|---|---|---|---|---|---|---|---|---|---|
| 1 | 95.75 | 1.36 | 0.45 | 0.40 | 0.27 | 0.00 | 0.01 | 0.00 | 0.02 | 0.28 |
| 2 | 96.34 | 1.31 | 0.29 | 0.06 | 0.24 | 0.00 | 0.00 | 0.03 | 0.00 | 0.00 |
| 3 | 97.37 | 0.99 | 0.43 | 0.20 | 0.56 | 0.38 | 0.01 | 0.02 | 0.00 | 0.15 |
| Rutile | $SiO_2$ | $Al_2O_3$ | $P_2O_5$ | MgO | CoO | NiO | CaO | $Na_2O$ | $Ta_2O_5$ | Total |
| 1 | 0.30 | 0.28 | 0.30 | 0.00 | 0.07 | 0.00 | 0.00 | 0.02 | 0.06 | 99.34 |
| 2 | 0.00 | 0.00 | 0.04 | 0.23 | 0.09 | 0.26 | 0.10 | 0.12 | 0.00 | 99.12 |
| 3 | 0.33 | 0.05 | 0.00 | 0.00 | 0.00 | 0.00 | 0.04 | 0.00 | 0.00 | 100.55 |

Table 2
Binding energy of Ti 2p and V $2p_{3/2}$ peaks of untreated, heated, quenched and irradiated rutile and the concentration of various atoms on the surface$_{XPS}$ (%)

| Rutile | Binding energy (eV) | | | Atom percentage$_{XPS}$ (%) | | | | |
|---|---|---|---|---|---|---|---|---|
| | Ti $2p_{3/2}$ | Ti $2p_{1/2}$ | V $2p_{3/2}$ | Ti | O | V | O/Ti | V/Ti |
| Untreated | 458.5 | 464.3 | 517.7 | 13.9 | 82.8 | 3.3 | 5.9 | 0.2 |
| Heated | 458.6 | 464.3 | 517.6 | 11.3 | 84.8 | 3.9 | 7.5 | 0.4 |
| Quenched | 458.8 | 464.5 | 517.6 | 10.1 | 85.8 | 4.1 | 8.5 | 0.4 |
| Irradiated | 458.8 | 464.5 | 517.8 | 11.9 | 84.6 | 3.5 | 7.1 | 0.3 |

Because the V $2p_{1/2}$ peak overlaps partly the O 1s peak [29] and the rutile contains low V concentration, the V $2p_{1/2}$ peak is hardly observed [30]. Thus only the V $2p_{3/2}$ peak was discussed (Fig. 1). The binding energies of V $2p_{3/2}$ peak range from 517.6 to 517.8 eV (Table 2), corresponding to $V^{5+}$ state [26].

A typical O 1s peak of pure $TiO_2$ is sharp and symmetric with a binding energy around 530 eV [31]. Due to overlapping by water adsorption peak, the O 1s peaks become asymmetric (Fig. 2). Ong et al. [32] pointed out that the high-energy part of O 1s peak is caused by broad water adsorption peak. The broad O 1s peaks can be deconvoluted into three peaks at 530.3, 531.8 and 533.2 eV (Fig. 2), which are corresponding to $O^{2-}$ in titanium oxides, dissociative adsorbed water $OH^-$, and adsorbed molecular water $H_2O$, respectively [33]. The percentages of $O^{2-}$, $OH^-$ and $H_2O$ peaks are given in Table 3. The concentrations of adsorbed water ($OH^-$ and $H_2O$) on the surface of the heated and quenched rutiles were higher than $O^{2-}$ concentration. The percentage of adsorbed water on the rutile

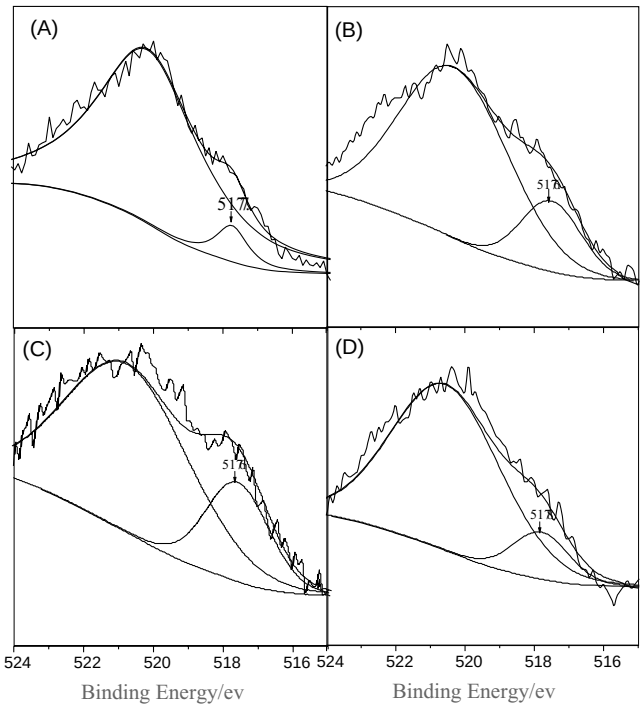


Fig. 1. V $2p_{3/2}$ peaks of untreated (A), heated (B), quenched (C) and irradiated (D) rutiles.

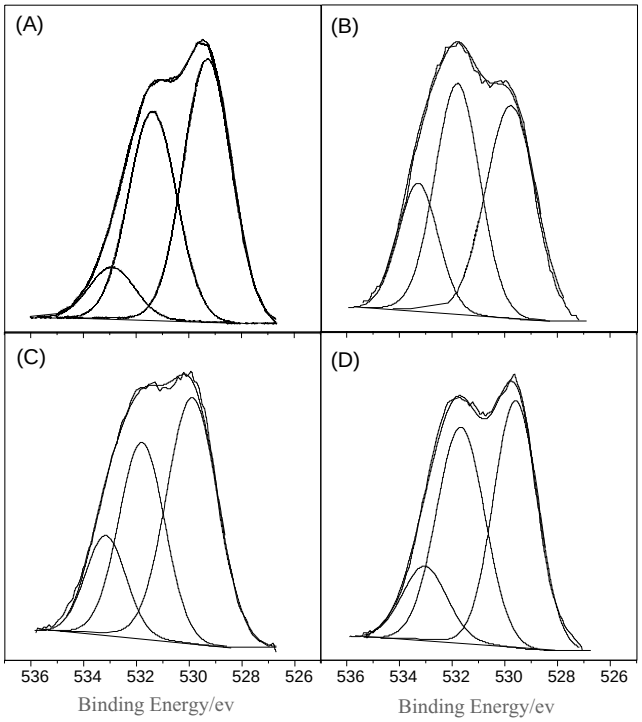


Fig. 2. Broad O 1s peak and the deconvoluted $O^{2-}$, $OH^-$, and $H_2O$ peaks for untreated (A), heated (B), quenched (C) and irradiated (D) rutiles.

surface was increased from 50.40 to 58.52% after quenching. While the percentage of adsorbed water on the surface of electron-irradiated rutile was decreased from 50.40 to 47.94%.

The integrate areas of Ti 2p, V 2p and O 1s peaks of rutile were computed and the corresponding atom concentration ($C_x$) were calculated with atom sensitivity factor (ASF) equation [34]:

$$C_x = \frac{n_x}{\sum_i n_i} = \frac{I_x/S_x}{\sum_i I_i/S_i} \quad (2)$$

Table 3
Percentages of $O^{2-}$, $OH^-$ and $H_2O$ on the surfaces of untreated, heated, quenched and irradiated rutiles

| Rutile | $O^{2-}$ (%) | $OH^-$ (%) | $H_2O$ (%) | $H_2O + OH^-$ (%) |
|---|---|---|---|---|
| Untreated | 49.6 | 41.2 | 9.2 | 50.4 |
| Heated | 43.9 | 42.3 | 13.8 | 56.1 |
| Quenched | 41.5 | 37.8 | 20.7 | 58.5 |
| Irradiated | 52.1 | 29.4 | 18.5 | 47.9 |

Table 4
Degradation of halohydrocarbons with and without rutiles

| Time (h) | Trichloroethylene (%) | | | Tetrachloroethylene (%) | |
|---|---|---|---|---|---|
| | No rutile | Untreated rutile | Electron irradiation | No rutile | Untreated rutile |
| 0 | 0 | 0 | 0 | 0 | 0 |
| 1 | 39 | 83 | 65 | 41 | 94 |
| 2 | 50 | 91 | 81 | 62 | 97 |
| 3 | 65 | 97 | 88 | 81 | 99 |
| 4 | 68 | 99 | 94 | 89 | 100 |

Table 5
Degradation of halohydrocarbons with heated rutiles

| Time (min) | Tetrachloroethylene (%) | | Trichloroethylene (%) | |
|---|---|---|---|---|
| | Untreated rutile | Rutile heated at 1273 K | Untreated rutile | Rutile heated at 1273 K |
| 0 | 0 | 0 | 0 | 0 |
| 20 | 67 | 74 | 72 | 86 |
| 40 | 80 | 91 | 89 | 98 |
| 60 | 89 | 98 | 99 | 100 |

Table 6
Degradation of halohydrocarbons with quenched rutiles

| Time (min) | Untreated | | 973 K | | 1073 K | | 1173 K | | 1273 K | | 1373 K | |
|---|---|---|---|---|---|---|---|---|---|---|---|---|
| | a | b | a | b | a | b | a | b | a | b | a | b |
| 0 | 0 | 0 | 0 | 0 | 0 | 0 | 0 | 0 | 0 | 0 | 0 | 0 |
| 20 | 43 | 55 | 41 | 50 | 56 | 58 | 49 | 61 | 77 | 79 | 90 | 90 |
| 40 | 77 | 78 | 70 | 81 | 80 | 84 | 76 | 87 | 93 | 94 | 95 | 95 |
| 60 | 82 | 88 | 87 | 91 | 85 | 89 | 83 | 91 | 95 | 96 | 95 | 96 |

a: degradation of trichloroethylene (%), b: degradation of tetrachloroethylene (%). The degradation time of the quenched rutile at 1373 K is 34, 50 and 68 min, respectively.

where $S_x$ is ASF for a certain atom and $I_x$ is peak intensity (integrate area); $S_i$ is ASF of the $i$th atom and $I_i$ is its peak intensity. The calculated $C_x$ shows that heating, quenching and electron irradiation increased V and O concentrations on the rutile surface (Table 2).

### 3.3. Degradation by rutile

*Untreated rutile samples*. Degradation rate of trichloroethylene without rutile is less than 70% after a few hours of light irradiation. However, the degradation rate increased to 95% after adding rutile. Tetrachloroethylene shows similar behavior after adding rutile (Table 4). These examples indicate that the untreated rutile shows photoactivity.

*Heated rutile*. By using heated rutile for one hour, degradation rate of tetrachloroethylene reaches 98% and its concentration is less than 5 μg/l, meeting China's national discharge standard for pollutants [35]. The degradation rate of tetrachloroethylene with untreated rutile is less than 90% (Table 5). For trichloroethylene, degradation rate with heated rutile is also higher than that with untreated rutile. For example, after using heated rutile for 20 min, degradation rate of trichloroethylene is more than 85%; and the degradation rate with untreated rutile is only about 70% (Table 5). These results demonstrate that, compared to untreated rutile, the heated rutile further improves degradation rates of tetrachloroethylene and trichloroethylene.

*Quenched rutile*. Quenched rutile increases degradation rates of tetrachloroethylene and trichloroethylene as well. Table 6 lists degradation rates of tetrachloroethylene and trichloroethylene after using rutile quenched at different temperatures for certain time durations. Rutiles quenched at different temperatures result in different degradation rates. For trichloroethylene, the use of the rutile quenched at 1273 and 1373 K leads to degradation rates of more than 90% after 40 min; while the use of rutile quenched at lower temperatures leads to degradation rates of about 85% after 60 min, similar to degradation rates by using untreated rutile. Therefore, rutile quenching at 1273 and 1373 K improves the degradation rate of tetrachloroethylene and trichloroethylene most significantly (Figs. 3 and 4).

*Electron-irradiated rutile*. The degradation rates of trichloroethylene with electron-irradiated rutile were shown in Table 4. After the first hour of the experiment with electron-irradiated rutile, trichloroethylene had a degradation rate of 65%, lower than 83%, the degradation rate with untreated rutile. Thus, electron-irradiated rutile actually lowers degradation rate of trichloroethylene.

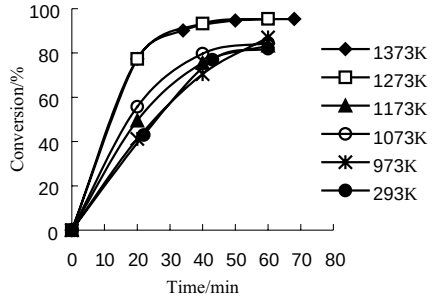


Fig. 3. Degradation of trichloroethylene by quenched rutiles.

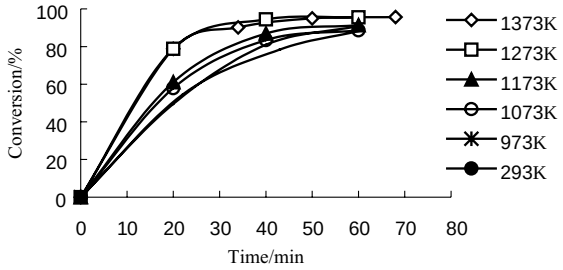


Fig. 4. Degradation of tetrachloroethylene by quenched rutiles.

## 4. Discussion

### 4.1. Effects of vanadium

Unlike pure synthetic rutile that lacks photoactivity [19], natural V-bearing rutile shows certain photoactivity. This is because that the substitution of V for Ti causes distortion of coordination polyhedra, increases structural microstrain [24,25], and creates structural vacancies [24]. During photocatalysis, the structural vacancies on the rutile surface absorb significant amount of $OH^- + H_2O$ (Table 3), which prevent photo-generated electron–hole pairs from combination, thus rutile's photoactivity is enhanced.

### 4.2. Effects of heating, quenching and electron irradiation

The XPS analyses showed that treatments, such as heating, increase V and O concentrations on the surface of rutile (Table 2). Therefore, on the surface of treated rutiles, more $V^{5+}$ replaces $Ti^{4+}$ and more positive charges are created. In addition, water dissociation into $OH^- + H^+$ is energetically feasible at the defect sites [36,37]. In order to neutralize the positive charges on the rutile's surface, negatively charged hydroxyl $OH^-$ is absorbed on the rutile's surface. The hydroxyl ions on the rutile's surface further enhance the photocatalytic activity of rutile [14]. Among rutiles treated by heating, quenching and electron irradiation, quenched rutile has the most adsorbed water and V on its surface, heated rutile has moderate amounts of adsorbed water and V on its surface, and electron-irradiated rutile do not increase adsorbed water and V concentrations on its surface.

Adsorbed water and hydroxyl groups on rutile surface play a crucial role at the initial stage of photocatalysis [38,39]. The hydroxyl combines with photo-generated holes and form strongly oxidizing radical OH, which prevents electron–hole pairs from recombination [40]. Rutiles treated by heating and quenching contain high concentrations of adsorption water ($OH^-$ and $H_2O$) on the surface. Therefore, these rutiles have higher phototactivity. The inferior catalytic effect of the electron-irradiated rutile might be caused by decomposition of $OH^-$ by reactions $OH^- \rightarrow H^+ + O^{2-}$ and $H^+ + e \rightarrow (1/2)H_2 \uparrow$ [33].

## 5. Conclusions

Natural V-bearing rutile shows photocatalytic property due to V substitution for Ti in rutile structure. Treatments by heating and quenching increase structural vacancies and V and O concentrations on rutile surface and cause more $OH^-$ be adsorbed on rutile surface, which in turn improve rutile's photocatalytic ability in degradation of halohydrocarbons.

The use of rutile heated at 1273 K for degradation of trichloroethylene showed that, after 1 h, the concentration of trichloroethylene decreased to less than 5 μg/l, meeting China's national discharge standard for organic waste water. Similarly, by using rutile quenched at 1273 and 1373 K for degrading trichloroethylene, low concentrations of trichloroethylene can also be obtained. This study also demonstrated that electron irradiation fails to improve rutile's photocatalytic ability in degradation of halohydrocarbons.

## Acknowledgements

This work was supported by the National Key Program for Basic Research of China (No. 2001CCA02400) and by the National Science Foundation of China (Grant No. 40172022). We thank the constructive comments from two reviewers.

## References

[1] O.M. Alfano, D. Bahnemann, A.E. Cassano, R. Dillert, R. Goslich, Catal. Today 58 (2000) 199.
[2] A. Fujishima, K. Honda, Nature 238 (1972) 37.
[3] D.S. Muggli, L. Ding, Appl. Catal. B: Environ. 32 (2001) 181.
[4] A.J. Maira, K.L. Yeung, J. Soria, J.M. Coronado, C. Belver, C.Y. Lee, V. Augugliaro, Appl. Catal. B: Environ. 29 (2001) 327.
[5] A. Lu, Acta Petrol. Miner. 22 (4) (2003) 323.
[6] R.T. Shuey, Semiconducting Ore Minerals, Elsevier, Amsterdam, 1975.
[7] T.D. Waite, in: M.F. Hochella Jr., A.F. White (Eds.), Mineral–Water Interface Geochemistry, Review in Mineralogy, Mineralogical Society of America, 1990, p. 559.
[8] A. Fujishima, T.N. Rao, D.A. Tryk, J. Photochem. Photobiol. C: Photochem. Rev. 1 (2000) 4.

[9] R. Benedix, F. Dehn, J. Quaas, M. Orgass, Leipzig Annual Civil Engineering Report No. 5, Institut für Massivbau und Baustofftechnologie, Leipzig, 2000, p. 161.
[10] C. Wang, T. Wang, S. Zheng, Phys. E 14 (2002) 242.
[11] Y. Muraoka, T. Yamauchi, Y. Ueda, Z. Hiroi, J. Phys.: Condens. Matter 14 (2002) 757.
[12] T. Ohno, F. Tanigawa, K. Fujihara, S. Izumi, M. Matsumura, J. Photochem. Photobiol. A: Chem. 127 (1999) 107.
[13] K.T. Ranjit, H. Cohen, I. Willner, S. Bossmann, A.M. Braun, J. Mater. Sci. 34 (1999) 5273.
[14] J.C. Yu, L. Jun, R.W.M. Kwok, J. Photochem. Photobiol. A: Chem. 111 (1997) 201.
[15] W. Choi, A. Termin, M.R. Hoffman, J. Phys. Chem. 98 (1994) 13669.
[16] J. Lin, J.C. Yu, D. Lo, S.K. Lam, J. Catal. 183 (1999) 372.
[17] S. Chen, Y. Tao, Acta Sci. Nat. Univ. Nankaiensis 31 (1998) 79.
[18] D. Huang, Y. Gong, B. Liu, Q. Zhao, X. Zhao, J. Wuhan, Univ. Technol. 24 (2002) 1.
[19] Y. Nakaoka, Y. Nosaka, J. Photochem. Photobiol. A: Chem. 110 (1997) 302.
[20] A. Sclafani, L. Palmisano, M. Schiavello, J. Phys. Chem. 94 (1990) 829.
[21] K. Tanaka, T. Hisanaga, A.P. Rivera, in: D.F. Ollis, H. Al-Ekabi (Eds.), Photocatalytic Purification and Treatment of Water and Air, Elsevier Science, Lausanne, 1993, p. 169.
[22] A. Lu, Acta Petrol. Mineral. 20 (2001) 377.
[23] D. Rao, Silicate Physical Chemistry (Revision), Metallurgy Industry Publication Company, Beijing, 1996, p. 78.
[24] L.E. Depero, P. Bonzi, M. Musci, C. Casale, J. Solid State Chem. 111 (1994) 252.
[25] L.E. Depero, J. Solid State Chem. 103 (1993) 529.
[26] C.D. Wagner, Handbook of X-ray Photoelectron Spectroscopy, Perkin-Elmer Corporation, Physical Electronics Division, Eden Prairis, 1979, p. 55344.
[27] N.J. Price, J.B. Reitz, J.R. Madix, E.I. Solomon, J. Electr. Spectrosc. Relat. Phenom. 98/99 (1999) 259.
[28] P.M. Kumar, S. Badrinarayanan, M. Sastry, Thin Solid Films 358 (2000) 127.
[29] D. Robba, D.M. Ori, P. Sangalli, G. Chiarello, L.E. Depero, F. Parmigiani, Surf. Sci. 380 (1997) 315.
[30] D.A. Bulushev, L. Kiwi-Minsker, F. Rainone, A. Renken, J. Catal. 205 (2002) 118.
[31] M.M. Rahman, K.M. Krishna, T. Soga, T. Jimbo, M. Umeno, J. Phys. Chem. Solids 60 (1999) 209.
[32] J.L. Ong, L.C. Lucas, G.N. Raikar, J.C. Gregory, Appl. Surf. Sci. 72 (1993) 7.
[33] T. Lu, L. Lin, C. Zhao, Nucl. Instrum. Meth. Phys. Res. B 141 (1998) 457.
[34] S. Liu, D. Wang, C. Pan, Analysis of XPS Spectrum, Science Press, Beijing, 1988, p. 93.
[35] Integrated wastewater discharge standard of PR China, GB 8978-1996. http://www.cepsn.com/hbbz.htm.
[36] T. Bredow, K. Jug, Surf. Sci. 327 (1995) 407.
[37] M.A. Henderson, Surf. Sci. 355 (1996) 166.
[38] Z. Ding, G.Q. Lu, P.F. Greenfield, J. Phys. Chem. B 104 (2000) 4815.
[39] E.V. Stefanovich, T.N. Truong, Chem. Phys. Lett. 299 (1999) 623.
[40] J.C. Yu, J. Yu, W. Ho, J. Zhao, J. Photochem. Photobiol. A: Chem. 148 (2002) 331.